

Linköping Studies in Science and Technology
Dissertation No.1519

Reactive High Power Impulse Magnetron Sputtering of Metal Oxides

Montri Aiempanakit

Plasma & Coatings Physics Division
Department of Physics, Chemistry and Biology
Linköping University, Sweden

ISBN: 978-91-7519-622-0

ISBN 0345-7524

Printed by LiU-Tryck, Linköping, Sweden 2013

Abstract

The work presented in this thesis deals with reactive magnetron sputtering processes of metal oxides with a prime focus on high power impulse magnetron sputtering (HiPIMS). The aim of the research is to contribute towards understanding of the fundamental mechanisms governing a reactive HiPIMS process and to investigate their implications on the film growth.

The stabilization of the HiPIMS process at the transition zone between the metal and compound modes of Al-O and Ce-O was investigated for realizing the film deposition with improved properties and higher deposition rate and the results are compared with direct current magnetron sputtering (DCMS) processes. The investigations were made for different sputtering conditions obtained by varying pulse frequency, peak power and pumping speed. For the experimental conditions employed, it was found that reactive HiPIMS can eliminate/suppress the hysteresis effect for a range of frequency, leading to a stable deposition process with a high deposition rate. The hysteresis was found to be eliminated for Al-O while for Ce-O, it was not eliminated but suppressed as compared to the DCMS. The behavior of elimination/suppression of the hysteresis may be influenced by high erosion rate during the pulse, limited target oxidation between the pulses and gas rarefaction effects in front of the target. Similar investigations were made for Ti-O employing a larger target and the hysteresis was found to be suppressed as compared to the respective DCMS, but not eliminated. It was shown that the effect of gas rarefaction is a powerful mechanism for preventing oxide formation upon the target surface. The impact of this effect depends on the off-time between the pulses. Longer off-times reduce the influence of gas rarefaction.

To gain a better understanding of the discharge current-voltage behavior in a reactive HiPIMS process of metal oxides, the ion compositions and ion energy distributions were measured for Al-O and Ti-O using time-averaged and time-resolved mass spectrometry. It was shown that the different discharge current behavior between non-reactive and reactive modes couldn't be explained solely by the change in the secondary electron emission yield from the sputtering target. The high fluxes of O^{1+} ions contribute substantially to the discharge current giving rise to an increase in the

discharge current in the oxide mode as compared to the metal mode. The results also show that the source of oxygen in the discharge is both, the target surface (via sputtering) as well as the gas phase.

The investigations on the properties of HiPIMS grown films were made by synthesizing metal oxide thin films using Al-O, Ti-O and Ag-Cu-O. It was shown that Al₂O₃ films grown under optimum condition using reactive HiPIMS exhibit superior properties as compared to DCMS. The HiPIMS grown films exhibit higher refractive index as well as the deposition rate of the film growth was higher under the same operating conditions. The effect of HiPIMS peak power on TiO₂ film properties was investigated and the results are compared with the DCMS. The properties of TiO₂ films such as refractive index, film density and phase structure were experimentally determined. The ion composition during film growth was investigated and an explanation on the correlation of the film properties and ion energy was made. It was found that energetic and ionized sputtered flux in reactive HiPIMS can be used to tailor the phase formation of the TiO₂ films with high peak powers facilitating the rutile phase while the anatase phase can be obtained using low peak powers. These phases can be obtained at room temperature without external substrate heating or post-deposition annealing which is in contrast to the reactive DCMS where both, anatase and rutile phases of TiO₂ are obtained at either elevated growth temperatures or by employing post deposition annealing. The effect of HiPIMS peak power on the crystal structure of the grown films was also investigated for ternary compound, Ag-Cu-O, for which films were synthesized using reactive HiPIMS as well as reactive DCMS. It was found that the stoichiometric Ag₂Cu₂O₃ can be synthesized by all examined pulsing peak powers. The oxygen gas flow rate required to form stoichiometric films is proportional to the pulsing peak power in HiPIMS. DCMS required low oxygen gas flow to synthesis the stoichiometric films. The HiPIMS grown films exhibit more pronounced crystalline structure as compared to the films grown using DCMS. This is likely an effect of highly ionized depositing flux which facilitates an intense ion bombardment during the film growth using HiPIMS. Our results indicate that Ag₂Cu₂O₃ film formation is very sensitive to the ion bombardment on the substrate as well as to the back-attraction of metal and oxygen ions to the target.

Populärvetenskaplig sammanfattning på svenska

Arbetet som presenteras i denna avhandling berör beläggning på ytor av material med hjälp av reaktiv sputtering. Speciellt används en teknik kallad "high power impulse magnetron sputtering" (HiPIMS) på svenska ungefär högeffektpulsad magnetron sputtering och avhandlingen utreder hur den påverkar den reaktiva sputterprocessen och tillväxten av skikten. Avhandlingens arbetet har syftat både till att erhålla en grundläggande förståelse av den reaktiva sputteringsprocessen t.ex., hur den reaktiva gasen påverkar ström-spännings-karakteristiken hos de pålagda pulserna och jonsammansättningen i plasmat, samt till att använda den erhållna förståelsen för att tillverka skikt av föreningar, speciellt metalloxider. Normalt är reaktiva sputterprocesser väldigt ostabila när man blandar in den reaktiva gasen för att få rätt sammansättning på beläggningen. Hur olika parametrar, såsom pulsfrekvens, pulseffekt och gasflöde hastighet genom systemet, påverkar denna instabilitet har undersöktes. I detta arbete visar jag att det går att stabilisera processen med hjälp av HiPIMS och jag föreslår möjliga mekanismer för hur denna stabilisering går till. Dessa inkluderar en kombination av hög etshastighet av sputterkällan under pulserna, begränsad oxidering av sputterkällan mellan pulserna och av gasurtunning framför sputterkällan. I avhandlingen visas att beläggningar av Al_2O_3 kan växas med hjälp av reaktiv HiPIMS och få egenskaper som är överlägsna skikt växta med traditionell reaktiv sputtering. Dessa egenskaper inkluderar högre tillväxthastighet, tätare material och högre brytningsindex. Ett annat material som studerats är TiO_2 , ett material som används som en optisk ytbeläggning för att erhålla olika optiska fenomen men också för att materialet är fotokatalytiskt vilket kan hålla en yta ren om den utsätts för solljus. Beroende på vilka egenskaper man vill optimera så vill man kunna använda olika faser av TiO_2 . När man växer material med HiPIMS så kan man nyttja de skapade jonerna för att bombardera skiktet under tillväxt. Med hjälp av detta jonbombardemang kan önskad fas erhållas. Ett tredje material som studerades är silverkopparoxid. Det är ett material som kan finna tillämpningar som solcellsmaterial. Det visade sig att skikt som växtes med HiPIMS har en bättre kristallinet (färre gitterdefekter och större korn). Detta är av stor vikt för solcellstillämpningen.

Preface

This doctoral thesis is a part of my Ph.D. studies (March 2008 to 2013) carried out in the Plasma & Coatings Physics Division of the Department of Physics, Chemistry and Biology (IFM) at Linköping University. The aim of my research is to: (i) understand the mechanisms in reactive high power impulse magnetron sputtering (HiPIMS) processes via HiPIMS parameters and (ii) demonstrate the possibility to grow high quality metal oxide films without using a feedback control system. The results are presented in several of my papers and at the end of this thesis.

This research is financially supported by the Swedish Research Council (VR), the Strategic Research Center in Materials Science for Nanoscale Surface Engineering (MS²E) and the Ministry of Science and Technology, Thailand.

Linköping, April 2013

Included Papers

Fundamentals of reactive high power impulse magnetron sputtering

Paper 1

“Hysteresis and process stability in reactive high power impulse magnetron sputtering of metal oxides”

M. Aiempnanakit, T. Kubart, P. Larsson, K. Sarakinos, J. Jensen and U. Helmersson
Thin Solid Film **519** (2011) 7779-7784.

Paper 2

“Studies of hysteresis effect in reactive HiPIMS deposition of oxides”

T. Kubart, M. Aiempnanakit, J. Andersson, T. Nyberg, S. Berg and U. Helmersson
Surface & Coatings Technology **205** (2011) S303–S306.

Paper 3

“Understanding the discharge current behavior in reactive high power impulse magnetron sputtering of oxides”

M. Aiempnanakit, A. Aijaz, D. Lundin, U. Helmersson and T. Kubart
Journal of Applied Physics **113** (2013) 133302.

Growth using reactive high power impulse magnetron sputtering

Paper 4

“Effect of peak power in reactive high power impulse magnetron sputtering of titanium dioxide”

M. Aiempnanakit, U. Helmersson, A. Aijaz, P. Larsson, R. Magnusson, J. Jensen and T. Kubart
Surface & Coatings Technology **205** (2011) 4828–4831.

Paper 5

“Ag₂Cu₂O₃ films deposited by reactive high power impulse magnetron sputtering”

M. Aiempnanakit, E. Lund, T. Kubart and U. Helmersson
In manuscript

My contribution to included papers

In **Paper 1**, I planned and performed most experiments. I performed the SEM and XRD analyses and wrote the paper with the assistance of the co-authors.

In **Paper 2**, I performed most experiments (except for TRIDYN simulations) and contributed to the writing of the paper.

In **Paper 3**, I performed most experiments (except for TRIDYN simulations) and wrote the paper with the assistance of the co-authors.

In **Paper 4**, I planned and performed most experiments (except for spectroscopic ellipsometry and TOF-ERDA) and wrote the papers with the assistance of the co-authors.

In **Paper 5**, I planned and performed most experiments and wrote the paper with the assistance of the co-authors.

Acknowledgements

I would like to acknowledge the financial support I received from the **Department of Physics, Silpakorn University** and would like to thank the **Ministry of Science and Technology, Thailand** for providing me a Ph.D. scholarship, which has supported me during my study in Sweden.

I would like to express my sincere gratitude to my supervisor, **Professor Ulf Helmersson**, for giving me the opportunity to study at Linköping University, for his supervision, suggestions, discussions throughout the thesis, encouragement and giving me freedom to explore the field of reactive HiPIMS.

I wish to express special thanks to my co-supervisor, **Dr. Tomas Kubart**, for his guidance, ideas during this work and support during the entire PhD studies. Your experience with reactive sputtering was very helpful.

I would like to thank the co-authors of the papers for their valuable contributions.

I would like to thank my former colleagues in the Plasma & Coatings Physics Division including: **Erik Wallin** for training me to use the sputtering system Ginnungagap (GG) and guiding me to start the thesis; **Petter Larsson** for technical assistance and helpful discussions about the sputtering system, sample preparation, assistance in the machine workshop and good ideas; **Daniel Lundin** for good discussions and friendship; **Mattias Samuelsson** for good discussions and the wonderful midsummer celebrations.

I would like to thank all of my present colleagues in the Plasma & Coatings Physics Division including **Asim Aijaz** and **Daniel Magnfält** for the lively discussions and help in the lab, and **Dr. Kostas Sarakinos**, together with other colleagues in the group from who I have learned many things. I would like to thank **Sankara Pillay** for your efforts on correcting this thesis and giving good suggestions for the improvement.

I would like to thank **Mikael Amlé** for providing all administrative support.

I extend many thanks to my friends and colleagues in the Thin Film Physics and Nanostructured Materials Divisions and other co-workers at IFM, especially **Pakorn Preechaburana** and **Supaluck Amloy** for their encouragement.

I would like to thank **Thai friends and their families** in Sweden for making me feel like I'm in Thailand.

I also wish to thank **Promporn Wanwacharakul, Yuttapoom Puttisong** and **Satapana Onla** for guidance and continued support.

Finally, I wish to express my gratitude to my **parents, sisters** and **brothers** for their love, encouragement and support.

Contents

Abstract.....	iii
Populärvetenskaplig sammanfattning på svenska.....	v
Preface.....	vii
Included papers.....	ix
Acknowledgements.....	xi
1. Introduction	1
1.1 Thin film technology.....	1
1.2 Research background.....	2
1.3 Aims and objectives.....	3
1.4 Outline.....	3
2. Thin film deposition and growth	5
2.1 Plasma physics.....	5
2.2 Plasma for material processing.....	6
2.3 Sputter deposition.....	8
2.4 Magnetron sputtering.....	10
2.5 Magnetron sputtering - mode of operation.....	12
2.5.1 Direct current magnetron sputtering	12
2.5.2 High power impulse magnetron sputtering	13
2.6 Thin film growth.....	16
3. Reactive magnetron sputtering	19
3.1 General behavior.....	19
3.2 Growth of compound films	20
3.3 Process stability.....	21
3.3.1 Hysteresis effect.....	21
3.3.2 Arcing.....	25
3.3.3 Disappearing anode effect.....	26
3.4 Strategies to reduce hysteresis.....	26
3.5 Discharge current behavior in reactive HiPIMS discharge.....	29

4. Metal oxide thin film materials	31
4.1 Al-O system.....	31
4.2 Ti-O system.....	32
4.3 Ce-O system.....	32
4.4 Ag-Cu-O system.....	32
5. Plasma and film characterization	35
5.1 Plasma characterization.....	35
5.1.1 Mass spectrometry.....	35
5.2 Film characterization.....	37
5.2.1 X-ray diffractometry.....	37
5.2.2 Spectroscopic ellipsometry.....	39
5.2.3 Scanning electron microscope.....	40
5.2.4 Elastic recoil detector analysis.....	40
6. Summary of results	43
6.1 Fundamentals of reactive high power impulse magnetron sputtering....	43
6.2 Growth using reactive high power impulse magnetron sputtering.....	45
References.....	47
Paper 1.....	53
Paper 2.....	61
Paper 3.....	67
Paper 4.....	77
Paper 5.....	83

Chapter 1

Introduction

1.1 Thin Film Technology

Thin films are layers of materials which are typically deposited upon substrates. The thickness of these films is in the range of a few nanometers to a few micrometers [1, p. 3]. At this scale, the properties of thin films may differ significantly from bulk materials. Using thin films one can combine the properties of a bulk material with those of the surface material, which is formed as thin film and the overall effect is the improvement in the desired properties such as electrical, mechanical and optical properties. In addition to improving properties of a substrate material i.e., cutting tools, etc., thin films and coatings can also reduce the cost of materials compared to its bulk counterpart. Various materials including metals, dielectrics (insulator), semiconductors and polymers are widely used as thin films in various industrial applications such as electronic devices, optical coatings, etc. The film quality depends on the deposition technique used as well as process conditions during the deposition. There are a number of methods for producing thin films, such as chemical vapor deposition, evaporation, sputtering (atoms are ejected from a surface due to an impact of energetic particle on the surface; sputtering is the main technique of thin film deposition used in this thesis and it is described in detail in Chapter 2, section 2.3) and various combinations of these. Generally, these methods are divided into two main

groups: Chemical Vapor Deposition (CVD) and Physical Vapor Deposition (PVD) [2, p. 96].

In a CVD process, thin films are grown via chemical reactions of precursor gases taking place at high temperatures. The process has the capability of depositing a large variety of coatings of different materials (metals, semiconductors, organics and inorganics) on large area substrates [2, p. 278]. However, there are several limiting aspects of the CVD process, many of them related to the high process temperatures often required [2, p. 286].

In a PVD process, thin film deposition takes place via condensation of a vaporized material onto a substrate [2, p. 145]. The vapor of the source material can be generated by several means such as heating, ion bombardment, etc. The most common PVD methods are evaporation and sputtering. These methods allow for the deposition of thin films at low substrate temperature (below 100 °C). At present, the use of PVD is widely used in a wide range of industrial applications.

1.2 Research Background

Compound thin films such as metal oxides, nitrides, carbides and their combinations are widely used in various industrial applications. Today, we find products with compound films prepared by PVD based methods such as reactive magnetron sputtering, in areas such as protective coatings, smart windows, photovoltaic applications and microelectronic devices. New applications bring higher requirements on the stability of the growth process and on the performance (e.g., quality and efficiency) of deposition systems. Along with stability, the process should facilitate an accurate control over film composition, film properties and thickness uniformity while maintaining a high deposition rate. Moreover, the reproducibility and the portability of the process from one system to another are essential. There are several issues which are encountered during reactive deposition processes — especially with metal oxide systems which — that along with an efficient control, demand new solutions.

The hysteresis effect is one of the primary problems encountered during reactive sputtering and is caused by compound film formation at the surface of the sputtering target (target poisoning). This leads to process instability and sometimes a very low

deposition rate as the reactive gas flow increases [3–5]. An external feedback control system is commonly employed to overcome this issue; however, this adds an additional cost and complexity to the production process. Elimination or suppression of hysteresis without an external feedback control will facilitate low cost, high deposition rate film production with a stable process.

Recently, reactive magnetron sputtering of metal oxide thin films using high power impulse magnetron sputtering (HiPIMS) has shown the possibility for the elimination/suppression of the hysteresis effect without using an external feedback control signal during film deposition [6,7]. These compelling results provide opportunities for the development of new technologies to deposit metal oxide thin films. Moreover, HiPIMS allows for controlling the energy and direction of the deposition flux. These ion fluxes can be used to influence film growth processes and make films with superior properties (e.g., optical and mechanical) as compared to films deposited by conventional magnetron sputtering.

1.3 Aims and Objectives

The aim of this research has been to make the reactive HiPIMS process an industrially viable method for high rate and high quality depositions of metal oxide thin films. This is achieved by developing an understanding of the fundamentals of the reactive HiPIMS process by employing several metal oxides such as Al_2O_3 , CeO_2 , TiO_2 and $\text{Ag}_2\text{Cu}_2\text{O}_3$. An understanding of the process has been achieved by studying the behavior of the hysteresis effect and discharge parameters such as discharge current, discharge voltage, reactive gas flow rate, etc., as well as by analyzing the plasma chemistry and plasma energetic using mass spectrometry (under conditions suitable for thin film deposition). The properties of the deposited films have been investigated by employing several analytical techniques such as scanning electron microscopy (SEM), x-ray diffraction (XRD), spectroscopic ellipsometry (SE) and elastic recoil detection analysis (ERDA).

1.4 Outline

This thesis begins with a general overview of thin film deposition and growth as related to sputtering deposition techniques. Following this is a section on reactive magnetron sputtering in order to understand the general behavior and problems

encountered during reactive sputtering. Strategies to reduce hysteresis are suggested and the discharge current behavior in a reactive HiPIMS discharge is presented. A chapter on material systems studied in this thesis is included followed by a chapter on the characterization techniques used in this work. Finally, a summary of the results of the publications is provided.

Chapter 2

Thin Film Deposition and Growth

This chapter describes the basics of plasma-based thin film deposition techniques with a focus on magnetron sputtering based methods. First, the fundamentals of plasma physics and plasma discharges are presented followed by the introduction of magnetron sputtering and its commonly used variants. The general principles of thin film growth are also summarized in this chapter.

2.1 Plasma Physics

In 1929, Irving Langmuir [8] used the word “plasma” to describe the state of matter (ionized gas) inside the glow discharge. The plasma consists of positively and negatively charged species and neutral particles. Overall, plasma is neutral (quasi-neutrality) [1, p. 150-151] since there exists roughly an equal number of ions and electrons ($n_i = n_e = n$ particles/m³). Generally, we classify plasmas as thermal equilibrium and non-thermal equilibrium which are defined as:

1. *Thermal equilibrium Plasma*

In this type of plasma, the plasma constituents are in thermal equilibrium, i.e., the electron temperature is roughly equal to the ion temperature ($T_e = T_i$) [9, p. 8]. For example, much of matter in the universe (stars, etc.) consists of thermal equilibrium plasma [1, p. 159].

2. Non-thermal equilibrium Plasma

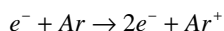
An example of non-thermal equilibrium plasmas is gas discharge at low pressure $P \approx 1$ mTorr to 1 Torr (0.13 - 133 Pa). In such plasmas, electrons have temperatures much higher than ions ($T_e \gg T_i$) [9, p. 8]. Due to their lower mass electrons exchange energy in collisions with the background gas less efficiently than ions. The temperature of ions is comparable with that of the container, whereas the electron temperature is in the order of several thousand degrees Kelvin [1, p. 159].

The plasma relevant for this thesis is of the low-pressure non-thermal equilibrium type which is generated via an electrical discharge of an inert gas. A brief description of the electrical gas discharges is presented in the next section.

2.2 Plasma for Material Processing

The plasma for material processing such as those used in PVD based glow discharge methods are generated via the electrical discharge of a gas under low pressure in an evacuated chamber. An inert gas (usually Ar) is used as a working gas. The electrical discharge is generated by applying an electrical voltage to the electrodes (cathode and anode) whereas the walls of the chamber (usually) serve as the anode. The gas discharge plasma can be divided into three different regimes which include *dark discharge*, *glow discharge* and *arc discharge* (see Figure 1) based on the discharge current [10].

Dark discharge: When an electrical potential is applied between the two electrodes, few electrons (present due to, e.g., background radiation) are accelerated towards the anode with a kinetic energy supplied by the difference in potential between the electrodes. Collisional processes — i.e., elastic and inelastic collision — between energetic electrons and neutral gas particles (gas atoms) can occur. If the electrons have sufficient energy, they can ionize neutral gas particles through inelastic collisions via the following reaction:



The resulting electrons can take part in further ionization of the gas atoms. Gas ions (Ar^+) will be accelerated towards the cathode and as a result of their impact, electrons (often called *secondary electrons*) along with the atoms of the cathode

material are ejected through the process of sputtering. The ejected atoms are, therefore, termed as the *sputtered atoms* (as explained in the following section). Initially, there is very small current flowing due to the low number of charge carriers. This regime is called the *Townsend discharge* [2, p. 149-150] (see Figure 1).

Glow discharge: If enough secondary electrons are ejected to generate the same number of ions that are used to generate the secondary electrons, the discharge is self-sustained. In this regime, gas breakdown occurs and the voltage decreases suddenly while the current increases rapidly. The plasma starts to glow and this regime is called the *normal glow* [2, p. 150]. Further increase in the voltage will result in a corresponding increase in the current density which will result in an increase in the discharge power. The ion bombardment will cover the whole cathode surface and at this point a transition to a new regime occurs which is called the *abnormal glow* [2, p. 150]. The process of sputtering (see section 2.3) belongs to the abnormal glow discharge.

Arc discharge: Increasing power density even further leads to thermionic emission of electrons from the cathode. The voltage drops suddenly while the current density becomes very high. This regime is called *arc discharge* [2, p. 150].

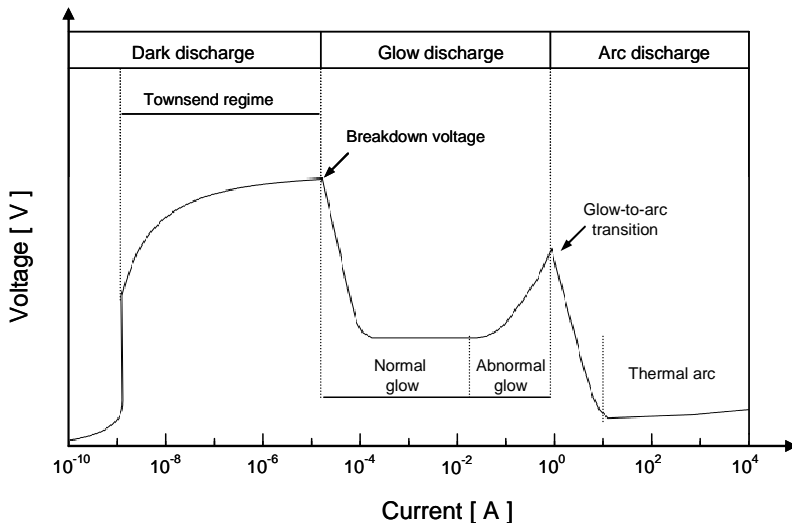


Figure 1. Different phases of plasma discharge generation. (After Roth [10].)

2.3 Sputter Deposition

Sputtering is a process in which atoms are ejected from a solid material (sputtering target) by bombarding the target surface with energetic particles, often ions of an ionized inert gas (sputtering gas) [2, p. 172].

A schematic drawing of a typical sputtering setup is presented in Figure 2. The sputtering target, usually solid, serves as the cathode by applying a negative voltage to it while the walls of the chamber serve as the anode. The chamber is evacuated using vacuum pumps after which an inert gas such as Ar is introduced to the chamber and the plasma is generated by an electrical discharge of the gas. The ions from the plasma bombard the target surface and sputter out atoms via momentum transfer [2, p. 174-180]. The rate of sputtering is proportional to the current density of inert gas ions bombarding the target surface [11]. The sputtered atoms traverse through the plasma and reach the substrate where they may condense and form films. Energy of the sputtered atoms is described by the so called Thomson energy distribution having an energy range of a few eV up to tens of eV. The number of sputtered atoms per incident ion, known as the *sputtering yield*, depends on the target material, surface binding energy of the target atoms, incident energy, mass of the projectile as well as on the angle of incidence of the bombarding particle [1, p. 566]. Moreover, during impact of the incident ion, there are other processes occurring as presented in Figure 3. For example, the emission of secondary electron from the target that is important to sustain the discharge as described in section 2.2 (Glow discharge). The number of emitted electrons per incident ion — known as *secondary electron yield* or *secondary electron emission coefficient* — also determines the discharge voltage [12].

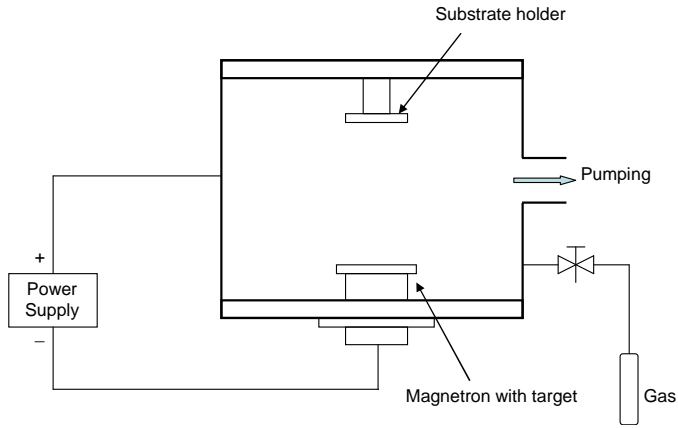


Figure 2. A schematics of a magnetron sputtering system.

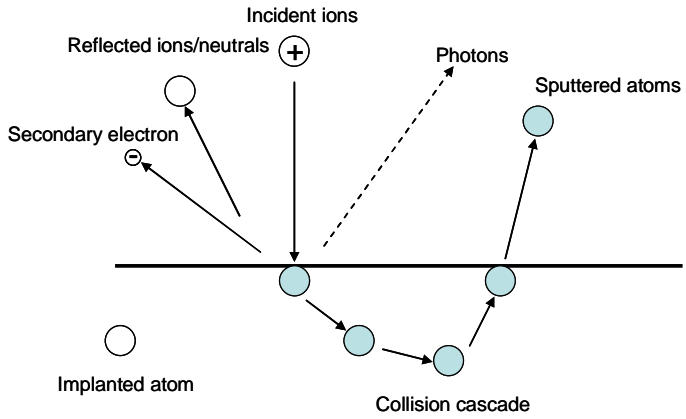


Figure 3. Different processes occurring during energetic incident ion bombardment.

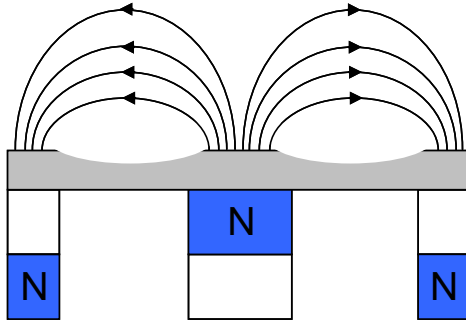
2.4 Magnetron Sputtering

Enhancing the ionization rate of gas ions during the process of sputtering to achieve more efficient sputtering conditions by a magnetic field is the concept used in magnetron sputtering [2, p. 222]. In this case, the magnets are placed behind the cathode in order to confine electrons close to the target surface using the magnetic field. The force acting on a charged particle in the presence of the magnetic field is the Lorentz force [9, p. 27] given by,

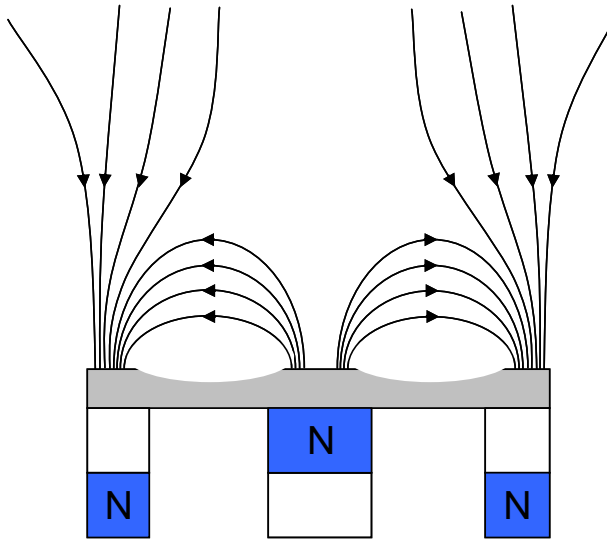
$$\vec{F} = q(\vec{E} + \vec{v} \times \vec{B}),$$

where q is the charge of particle, \vec{E} is electric field, \vec{v} is the velocity of charged particle and \vec{B} is the magnetic field. If the velocity of an electron is non-parallel to the magnetic field, it will experience force and follow helical path — which is also termed as the gyration radius — around the magnetic field lines. This increases the path and thus enhances the number of collisions between electrons and inert gas atoms leading to an increased ionization efficiency, which in turn increases the efficiency of the sputtering gas ion generation and thereby enhances the sputtering efficiency. Only the electrons are confined by the magnetic field. Ions due to their high masses have very large radius of the helical path comparable to the chamber dimension while the radius of gyration for electrons is typically about 1 mm [14, p. 46]. Plasma generated in magnetrons can be sustained at a lower pressure and lower operating voltage than in conventional diode sputtering where the sputtering efficiency is lower. In diode sputtering, since no magnetic field is used, high operating voltages and pressures are required to generate working gas ions. The typical operating pressure and discharge voltage used in magnetron sputtering — allowing the discharge to maintain — are 0.1 - 1 Pa and ~500 V, respectively, while those used in conventional sputtering are about 20 Pa and ~2 - 3 keV, respectively [13].

Circular planar magnetron is the most common magnetron configuration used. In this configuration, the magnet with one pole is placed at the central axis of the circular magnetron and the second pole is placed in the ring configuration around the outer edge, as shown in Figure 4.



(a)



(b)

Figure 4. Schematic of a cross section of a planar magnetron: (a) a balanced magnetron and (b) a type II unbalanced magnetron displaying only partial magnetic field lines close to the target surface. Here, the target appears with the characteristic racetrack formation.

In general, there are two standard types of magnetic field configuration used in deposition by magnetron sputtering [13]:

Balanced magnetron

The inner and outer magnets have the same strength which confines the electrons close to the target surface. This means that the plasma does not reach to the substrate and results in low ion bombardment of the substrate (ion current density $< 1 \text{ mAcm}^{-2}$) during film growth, thereby leading to low mobility of the depositing atoms on the substrate. This configuration is displayed in Figure 4 (a).

Unbalanced magnetron

If the inner magnet has a stronger pole than the outer magnet, the magnetic field configuration is unbalanced (type I unbalanced magnetron). In the type II configuration, the inner pole is weaker than the outer pole; the magnetic field lines open up and extend towards the substrate (see Figure 4 (b)). The electrons follow the field lines and, therefore, the plasma is also extended to the substrate. Ion bombardment (ion current density = 2 - 10 mAcm^{-2}) during growth can beneficially influence the film properties, such as increase coatings density and improve adhesion to the substrate.

2.5 Magnetron Sputtering - Modes of Operation

There are variants of magnetron sputtering depending on how the power is applied. Among these, the techniques used in this thesis are direct current magnetron sputtering and high power impulse magnetron sputtering.

2.5.1 Direct Current Magnetron Sputtering

In thin film sputtering deposition, direct current magnetron sputtering (DCMS) is successfully used to grow conducting thin films at high deposition rates whereas it can also be scaled for making large scale deposition of thin films. This makes DCMS an industrially attractive deposition technique. In DCMS, a constant power is applied to the target which is limited by the thermal load on the target. This power limitation (maximum power densities of a few 10s of Wcm^{-2}) does not allow for generating high plasma densities and the resulting ion fraction of the sputtered material is very low (only a few percent for metals) [15]. The majority of the flux is therefore consisting of neutral depositing species with energy of few eV. Overall, this results in the energy of

the sputtered species limiting the energy input into the substrate. It is possible to improve the film quality by applying a negative potential to the substrate, additional heat at the substrate and using an unbalanced magnetron (type II). This will provide the possibility of ion bombardment during film growth thereby improving the film quality.

2.5.2 High Power Impulse Magnetron Sputtering

A high power impulse magnetron sputtering (HiPIMS) discharge is operated with very high instantaneous power which facilitates the generation of high plasma densities, thereby creating highly ionized depositing fluxes. This scheme was introduced by Kouznetsov *et al.* [16] in 1999. In HiPIMS, the power to the cathode is applied using short uni-polar pulses of low duty cycle (pulse on-time divided by the period of the pulse) resulting in very high target peak power densities of the order of kWcm^{-2} [15–17]. The typical discharge current and voltage waveforms in HiPIMS are shown in Figure 5 (a).

Thanks to the high peak power, dense plasma is generated in front of the target with typical plasma densities in the order of 10^{19} m^{-3} . High electron density facilitates ionization of neutral species and a high degree of ionization of both gas and sputtered species is reached [16]. Ionized depositing fluxes provide the possibility to control their energy and direction during film growth [18,19]. The energetic bombardment during the film growth facilitates the growth of films with superior properties as compared to those obtained by conventional magnetron sputtering techniques, e.g., denser films [20–22], tailored film structures [15,21,23,24], good mechanical [22,24–26] and electrical [27] properties, etc.

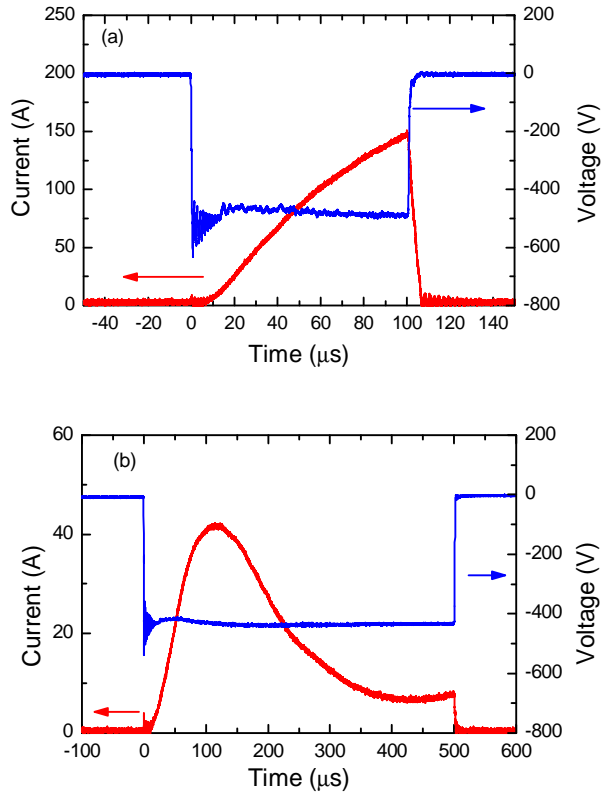


Figure 5. Discharge current and rectangular shape voltage waveforms generated by a HiPIMS power supply (SPIK 1000 A pulsing unit fed by an Advanced Energy Pinnacle generator). The data was recorded from an Ar – Ti HiPIMS discharge operating at the average power of 200 W with pulse on/off time configurations a) 100/19900 μs and b) 500/19500 μs .

Several researchers have investigated the current/voltage characteristic behavior of HiPIMS. Anders *et al.* [28] showed the current/voltage characteristic of a HiPIMS discharge using different target materials (Cu, Ti, Nb, C, W, Al and Cr). It was found that the HiPIMS current discharge exhibits two phases during the pulse on time. The initial phase depends on operating pressure and is dominated by gas ions. The second phase depends on the power and target materials; self-sputtering (the back-attraction of the sputtered atoms to the target and thereby causing sputtering) strongly contributes to the discharge current. Anders *et al.* [28] also showed that self-sputtering is significantly affected by the amount of the multiply charged sputtered ions rather than the singly charged ions. When the plasma discharge has a sufficient amount of

multiply charged ions of the sputtered material, these ions can be back attracted to the target giving rise to secondary electron emission which subsequently results in the transition of the discharge to the high current regime (see for example Figure 11 in [28]).

Besides bombardment of the target with the highly energetic positive gas ions, the kinetic energy from the ions transferred to the target also results in heat generated at the target surface. This heat can be transferred to the gas in front of the target. If we assume that the process gas obeys the ideal gas law, then the pressure of the gas (P_{gas}) can be given as,

$$P_{gas} = n_{gas}kT,$$

where k is the Boltzmann constant, n_{gas} is the gas density and T is the gas temperature. In the case that the gas pressure in the chamber is constant (Isobaric process), increased gas temperature leads to lower gas density (*gas dilution effect* or *gas rarefaction effect*) [29]. Moreover, the sputtered atoms also transfer energy to the gas atoms in front of the target via momentum transfer which means the gas density in front of the target surface is low which adds to the gas rarefaction. This phenomenon is also referred to as *sputtering wind* [30]. The magnitude of the gas rarefaction depends on several parameters [31], e.g., applied power, gas pressure and gas species. With HiPIMS plasma conditions — where the ionized particle density is very large — the effect of gas rarefaction is enhanced. Several researchers have investigated this phenomenon for HiPIMS as well as for Ionized PVD processes [17,28,29,31,32]. The decreased gas density in front of the target due to gas rarefaction results in the decrease of the sputtering gas ions which in turn causes a decrease in the discharge current [33] (see Figure 5 (b)). The effect of gas rarefaction and behavior of the discharge current for Ti and Al during the growth of Ti-O and Al-O have been discussed in **Paper 4**.

There are some disadvantages with HiPIMS, e.g. a lower deposition rate for metals as compared to conventional magnetron sputtering at the same average power. Helmersson *et al.* [15] reviewed deposition rate data in HiPIMS and found that the rates are typically 25 - 35% of the rates in DCMS. This observed low deposition rate can be attributed to several mechanisms, such as back-attraction of metal ions to the

target followed by self-sputtering [15,34,35] and anomalous transport of the sputtered species [36]. However, it is possible to increase the deposition rate by optimizing the parameters such as changing the magnetic field of the magnetron [37], applying a magnetic coil between the substrate and magnetron target [19].

2.6 Thin Film Growth

In the process of a film formation, atoms such as those sputtered from a target — in the case of magnetron sputtering — reach the substrate and condense to form a coating. There are several parameters that influence the growth behavior and structural features of thin films. These parameters are determined by the deposition conditions and influence how the atoms behave at the substrate before they are fully bonded to form films (referred to as *adatoms*) as well as the kinetics of the atoms (such as mobility, diffusion) at the substrate surface. The dependence of the structural features of thin films on the deposition conditions are often illustrated in the form of structure-zone diagrams, also known as structure zoned models (SZMs) [2, p. 497]. The first structure zone model for magnetron-sputtered metal thin films was proposed by Thornton [38]. The parameters that are used for describing the microstructural evolution of the films in this model are sputtering gas pressure and substrate temperature.

Sputtering gas pressure: Higher pressure means more frequent collisions of the sputtered atoms with the background gas and loss of energy. Therefore, the energy of the atoms arriving to the substrate is lower resulting in low adatom mobility giving films with a porous microstructure at low substrate temperature.

Substrate temperature: This represents the thermal effect on the film growth. Higher temperature of the substrate can enhance adatom mobility/diffusion which allows particles to find energetically favorable positions, resulting in formation of a film with larger grains (often columnar). At low temperature, the mobility/diffusion of adatom is very low, resulting in films with smaller grains or disordered structure. Low temperature films also contain more voids.

The SZM presented by Thornton is divided into four zones (1, T, 2 and 3) based on the resulting microstructure of the films influenced by the sputtering gas pressure and substrate temperature (in the SZM, the ratio of the substrate temperature and melting

point of the source material, i.e. T_s/T_m , has been used). The SZM is briefly discussed here:

1. Zone 1.

The structure of the films appear amorphous or of poor crystalline structure (many defects). The size of columns is typically tens of nanometers in diameter and the individual columns are separated by voided boundaries due to limited diffusion of adatoms on the surface. This zone occurs when the ratio T_s/T_m is in the range 0.1 - 0.5 and sputtering gas pressure is in the range 0.15 - 4 Pa.

2. Zone T.

Films in this zone contain poor crystalline structure similar to zone 1 but with no voids present. This zone may be considered as a transition between zones 1 and 2. The ratio T_s/T_m is in the range of 0.1 - 0.4 at sputtering gas pressure 0.15 Pa, and T_s/T_m is in the range 0.4 - 0.5 at sputtering gas pressure 4 Pa.

3. Zone 2.

In this zone crystalline columnar grain with fewer defects than in zone 1 are found. There are no voids (dense grain boundaries) between the columns. T_s/T_m is in the range 0.4 - 0.7 and atoms have energy high enough to diffuse on the surface.

4. Zone 3.

This zone occurs at $T_s/T_m > 0.6$, which is high enough to activate bulk diffusion in the film.

In addition, there are other parameters such as sputtering power, substrate bias, and deposition rate that influence the microstructure of films. However, the microstructure still falls within one of the SZMs proposed by Thornton and is determined by the energy of adatoms.

Chapter 3

Reactive Magnetron Sputtering

In this chapter, the fundamentals of a reactive magnetron sputtering process along with the discussion on elimination/suppression of the hysteresis effect are described.

3.1 General Behavior

Compound films such as metal oxides or metal nitrides are commonly deposited using an insulating compound target via radio frequency (RF) magnetron sputtering [2, p. 211]. However, the deposition rate is low because of the lower sputtering yield of the compound material relative to metal, especially in metal oxide. Also the sputtering efficiency in RF discharges is low. Another limitation of RF sputtering is its complicated and expensive hardware [3]. Therefore, RF magnetron sputtering is less attractive for industrial processes.

Reactive DC magnetron sputtering is an alternative technique for compound film deposition with potentially higher deposition rates than RF magnetron sputtering. Also, it uses metal targets which are easier and cheaper to manufacture. In a typical DCMS reactive process, compound film is synthesized in the presence of a reactive gas mixed with an inert working gas (e.g., Ar) by sputtering of a metallic target [2, p. 216]. Reactive gas in the discharge will react and form the desired compound at the substrate. For example, in the case of Al_2O_3 film growth, oxygen is introduced and

reacts with sputtered Al species to form Al_2O_3 on the substrate. In practice, however, there are some challenges which have to be addressed. Due to the process instability during reactive sputtering deposition, the deposition rates may be low. Also, the film stoichiometry may be influenced by the process conditions.

3.2 Growth of Compound Films

In reactive sputtering the sputtered material reacts with the reactive gas species and forms a compound. This offers the possibility to control the chemical composition and other film properties by varying the ratio between fluxes of the sputtered material and reactive gas.

For a typical reactive sputtering process, three different modes — metal mode, compound mode and the transition between them — are usually considered based on the reactive gas flow rate [4]. These modes are briefly discussed below.

1. Metal mode.

In this mode, the reactive gas flow fed into the chamber is not sufficient (reactive gas partial pressure is low) to react with all the sputtered material deposited at the surfaces in the chamber such as chamber walls, substrate and target. Thereby, the deposited film at the substrate is sub-stoichiometric and the desired properties of the film are not achieved due to the excess of target material (e.g. the composition corresponds to SiO_{2-x} , TiO_{2-x} or TiN_{1-x}). The sputtering target surface in this mode is predominantly metallic with a low fraction of compound.

2. Transition mode.

In this region, there is a complex dependence of the composition on the reactive gas flow typically there is more than one working point corresponding to a single value of the gas flow. Depending on the working point, the deposited films may be stoichiometric while the target surface is still metallic. The optimum working point, however, may be unstable.

3. Compound mode.

If the amount of the reactive gas is further increased the reactive gas partial pressure will be high and the whole target surface will be covered by the compound film (completely poisoned). This mode is referred to as compound mode. In this

region, the sputtering efficiency decreases which results in lower deposition rate as compared to the transition mode. This is a result of low sputtering yield of most compounds, especially oxides. In some cases, compound mode is preferred because of its stability, such as in large area coatings on glass. In addition to the low deposition rate, excess of reactive gas may result in over-stoichiometric composition of some compounds such as TiN with undesirable color.

3.3 Process Stability

During a reactive sputtering process, the reaction between the target material and the reactive gas might lead to process instability due to several effects [4]. The most common among these are: (1) Hysteresis (2) Arcing and (3) Disappearing anode.

3.3.1 Hysteresis Effect

The hysteresis effect is an issue to overcome in reactive sputtering in order to deposit stoichiometric films at a high deposition rate. If the discharge power is kept constant and the reactive gas flow is increasing, there will be a critical point in the reactive gas flow where the transition to compound mode occurs. At this critical point, the compound formation takes place at the whole surface of the sputtering target resulting in a sudden change in the sputtering rate as compared to the metal surface. Thereby, the deposition rate suddenly decreases. This is accompanied by an increase of reactive gas partial pressure. Typically, the sputtering yield of the compound is substantially lower than that of the elemental material [3–5]. This causes the deposition rate to decrease as the supply of the reactive gas increases which leads to a further decrease in the deposition rate and an avalanche like transition from metal to compound mode of operation. A typical experimental processing curve for the mass deposition rate vs. the supply of the reactive gas is shown in Figure 6. The mass deposition rate drops when the reactive gas flow is higher than the critical reactive gas flow. However, when decreasing the reactive gas flow the deposition rate does not increase at the same point but needs to be reduced more to show hysteresis in the gas flow [3–5]. The resulting curve is referred to as a *hysteresis curve*. The area between the decreasing and increasing points is referred to as the *hysteresis region*, sometimes also called *transition region*. At the same time, a corresponding hysteresis effect is observed in a plot of the reactive gas partial pressure vs. the reactive gas flow and this is shown in Figure 7. Hysteresis will also be observed for other process properties such as

discharge voltage and discharge current. This is because secondary electron yield also changes when the compound mode started which also affects the plasma impedance. The change of discharge voltage or discharge current (decrease or increase) as compared to the discharge voltage or discharge current in metal mode depends on the target material [12].

Controlling the reactive gas partial pressure instead of the reactive gas flow makes operation inside the transition region possible and leads to a hysteresis free [3,5]. A typical experimental processing curve for the reactive gas partial pressure vs. the supply of the reactive gas for a reactive sputtering process is shown in Figure 8 (a). The corresponding hysteresis effect is observed for the relationship between the mass deposition rate and the reactive gas flow and is shown in Figure 8 (b). In contrast to Figures 6 and 7, there is no hysteresis in the partial pressure in Figures 8 (a) and (b) and all operating points in the transition area are accessible. The partial pressure control requires active adjustments and the controller adds cost and complexity to the operation. However, it has substantial benefits. In this thesis, the hysteresis behavior has been investigated using reactive gas partial pressure control and is shown in **Paper 1**. Control of the reactive gas flow is discussed in **Paper 2**.

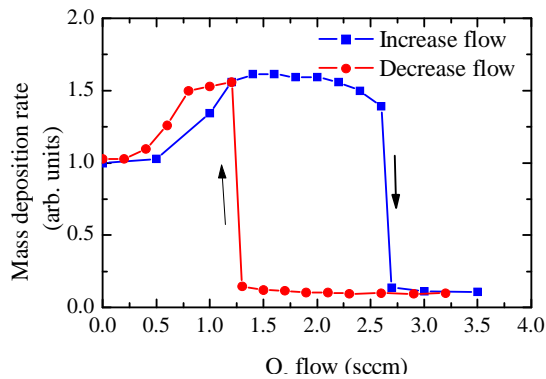


Figure 6. Typical experimental curve of mass deposition rate for reactive sputtering process of Ti.

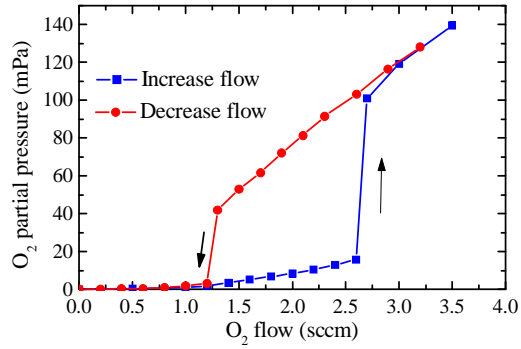


Figure 7. The partial pressure, P , of the reactive gas corresponding to the curve in Figure 6.

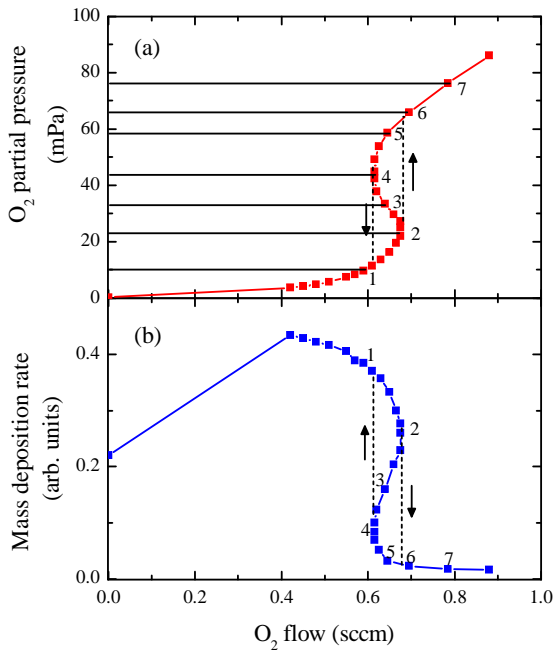


Figure 8. Diagram illustrating the process operates by controlling the O_2 partial pressure for the reactive sputtering of Al-O. (a) shows the general behavior for the O_2 partial pressure vs. O_2 gas flow and (b) shows mass deposition rate vs. O_2 gas flow. The example numbers indicated by 1, 2, ..., 7 in (a) correspond to points 1, 2, ..., 7 in (b)

As mentioned above, the sputtering yield of oxides is typically lower than that of metals, which means that sputtering from an oxide target results in lower deposition rates as compared to that of the metal mode. Large scale industrial processes require that films are grown at high deposition rates with a stable process. Higher deposition rates can be obtained by sputtering at a suitable point in the transition mode, thereby avoiding a fully poisoned target — using a process control based on a suitable feedback signal control to control the gas flow in order to keep the process stable. There are several quantities in reactive sputtering which can be used as a feedback signal for process control. Some types of signals are described in literature reviews [3,4] and references therein:

1. Optical emission spectrometer (OES) signal

When the partial pressure of the reactive gas increases, then the intensity of emission lines from the sputtered material decreases. This is due to an increasing fraction of the target surface covered by compound material which leads to a lower erosion rate. Schiller *et al.* [39] used the optical emission line of the target material as a feedback signal by adjusting the gas flow and were able to control the constant partial pressure of reactive gas during the deposition.

2. Mass spectrometer signal

Mass spectrometry measures the mass-to-charge ratio of charged particles and thus can analyze the chemical composition of the process atmosphere. Therefore, this technique provides a direct measure of the partial pressures (more details of mass spectrometry will be described in Chapter 5, section 5.1.1). Sproul and Tomashek [3] used mass spectrometry in order to maintain a constant partial pressure during the deposition. One issue with the mass spectrometer is that there is drift in signal intensity with time; however the ratio of peaks remains relatively constant with time, which can be used to compensate for this drift.

3. Cathode voltage signal

If the power (or current) is kept constant while changing the reactive gas flow, then the discharge voltage changes due to the change of the secondary electron yield of the target thus affecting the plasma impedance. Affinito and Parsons [40] used the feedback signal from the cathode voltage to stabilize the transition zone during deposition. However, this signal is not sensitive only to the partial pressure of reactive

gas but also to other parameters such as target thickness and temperature of the target that influence the cathode voltage. Therefore, using this feedback to synthesize a true stoichiometric film is difficult.

4. Oxygen sensor

An oxygen sensor is an electronic device which detects the concentration of oxygen. Typical oxygen sensor includes two porous electrodes, commonly platinum separated by a ceramic electrolyte such as yttria stabilized zirconia (YSZ) and semiconducting metal oxide (TiO_2 , CeO_2 , etc). One electrode is in contact with the ambient and the other in contact with the test gas environment. The oxygen molecules are adsorbed by electrode and dissociate into atomic oxygen. The electrons from electrolyte can transfer to oxygen atoms forming oxygen ions. The oxygen ions are collected by the electrodes creating a voltage difference between them. Such a sensor is used in various fields such as medical, food processing and automobiles [41]. The main use of oxygen sensors is in automobile engines in order to control the air-fuel ratio (Lambda , λ) in the combustion engine. This oxygen sensor is also referred to as *Lambda probe* [41]. Thereby, the oxygen sensor output is fed back to the engine control for controlling the engine operates around the stoichiometric point ($\lambda = 1$). In **Paper 1**, we used a lambda probe to detect the amount of oxygen introduced into the chamber. The potential measured by the lambda probe is send to the control unit and used to control oxygen gas mass flow controller in order to maintain the oxygen partial pressure. The advantage of using a lambda probe is the size and price, which makes it suitable for large area coating control systems with multiple sensors.

3.3.2 Arcing

In reactive sputtering of insulating films, arcing occurs on the target surface in the regions covered by non-conductive coatings. Positive charges will be collected at the non-conductive layer due to bombardment by positively charged ions. This charge can build up until the charge reaches the breakdown voltage and an arc will occur. There are many techniques, including RF power supply, a rotated cylindrical target [3,4], which are employed to avoid arcing. One commonly employed method of avoiding or significantly reducing the arcing effect during film deposition is to use pulsed DC reactive sputtering [42]. With this technique, an asymmetric bipolar pulsed voltage (the positive level is about only 10% of the negative peak level) is applied to the

cathode in order to allow for electrons to be attracted to the target surface to discharge the non-conductive layer.

3.3.3 Disappearing Anode Effect

Another commonly encountered problem in a reactive deposition process of insulating films is that insulating layers are also formed on the chamber walls (i.e., the walls serve as the anode for the discharge). This means the anode will gradually lose the ability to collect electrons, resulting in a shift of the plasma potential to a situation where the potential between the cathode and the plasma disappears and the plasma is extinguished. There are various methods to avoid the disappearing anode effect, for example, using dual magnetron sputtering [3,4].

3.4 Strategies to Reduce Hysteresis

In this thesis, we focus on the problem of hysteresis. Elimination or suppression of hysteresis could enable high rate sputtering without a feedback control unit which would be very beneficial. Berg and Nyberg [5] studied the parameters which influence the hysteresis effect by proposing a model for reactive sputtering. They discussed the dependence of the hysteresis on the gas pressure, deposition rate as well as reactive gas flow. The model also presented various ways to reduce or remove the hysteresis. Most of them, however, have limitations which prevent industrial use.

The examples of methods to reduce hysteresis in reactive sputtering are briefly summarized here:

1. Increasing pumping speed

Pumping speed is an important parameter that affects the hysteresis. Kadlec *et al.* [43] showed that if the pumping speed of the system (S_p) is greater than the critical pumping speed, the hysteresis effect can be avoided. In the model by Berg and Nyberg [5], it was shown that when the derivative of the total supply (sum of all sources for reactive gas consumption (Q_{tot}) and pressure (P)) is higher than zero $\left(\frac{dQ_{tot}}{dP} > 0\right)$, the hysteresis can be eliminated. However, the drawback of this method is the requirement for a very high pumping speed, especially for a large deposition system. For these reasons, the high pumping speed approach is not used very often.

2. Reduction of the target area

The area of the sputtering target also influences the hysteresis effect. Berg and Nyberg [5] showed that reducing the target area can reduce the width of hysteresis loop. Nyberg *et al.* [44] also showed corresponding experimental results. The problem of this method is the film uniformity which complicates deposition on large area substrates. However, they demonstrated that moving magnets inside the target assembly may be used.

3. Sub-stoichiometric target

Kubart *et al.* [45] have shown that the hysteresis effect can be removed by targets consisting of a mixture of compound and metal material (i.e., a fraction of composition between TiO_2 and Ti powders). They also shown a high deposition rate can be achieved when the target composition is optimized.

4. Gas composition

Severin *et al.* [46] suggested that for some metal oxide systems the addition of nitrogen gas into the sputtering atmosphere during reactive sputtering leads to stabilization of the process and the hysteresis effect can be eliminated. This is due to the higher sputtering yield of nitride than the sputtering yield of oxide. However, the deposited films contained low amounts of nitrogen.

5. Reactive HiPIMS

Initially, HiPIMS was used in reactive sputtering of metal nitrides for wear and corrosion resistant coatings (hard coating) as well as decorative coatings — e.g., CrN_x [22], TiN_x [47], etc. The deposited films show superior properties such as excellent adhesion, denser structure and higher hardness than films deposited by conventional PVD. In reactive HiPIMS of metal oxides, there are also improved film properties as compared to films deposited by conventional magnetron sputtering, e.g., films with a high refractive index [48,49], higher film density [48,50] and higher crystalline at lower deposition substrate temperature growth [51]. Achieving higher deposition rates in reactive HiPIMS vs. reactive DCMS is in contrast to results found in non-reactive sputtering (as previously discussed in section 2.5). This is due to the possibility to increase process stability during reactive deposition by HiPIMS [6,7]. However, the understanding of the mechanisms involved during reactive processes

using HiPIMS remains very limited. A brief review of the studies performed on the process stability when using reactive HiPIMS is presented below.

HiPIMS facilitates the elimination/suppression of the hysteresis. The first report on the hysteresis effect using HiPIMS and conventional DCMS on the Al-O system was presented by Wallin and Helmersson [6]. The work showed that HiPIMS can eliminate the hysteresis. The results demonstrated stabilization of the transition zone leading to true stoichiometric films with a high deposition rate. The authors suggested that the observed behavior is due to a high erosion rate during the pulses which can remove the compound film on the target surface. Furthermore, it might be an effect of limited target oxidation between the pulses and hence reduced target poisoning.

Another study of hysteresis in HiPIMS was published by Sarakinos *et al.* [7]. Zr-O system was used to investigate the hysteresis effect during reactive HiPIMS and DCMS. In that work the off-time was varied keeping the pulse on-time constant at 50 μs (off-time 450 μs and 1450 μs , corresponding with pulse frequency 2 kHz and ~666 Hz, respectively). The results showed that HiPIMS led to stabilization of the transition zone and also the deposition rate was higher than DCMS. The explanation was based on a high erosion rate of the compound film during the pulses. This is because of a higher discharge voltage in HiPIMS compared to DCMS resulting in higher sputtering yield. In general, HiPIMS uses higher discharge voltage to maintain the plasma than in DCMS and a longer off-time (lower frequency) needs a higher discharge voltage. They calculated sputtering yield of ZrO_2 based on the observed discharge voltage and found that a higher sputtering yield of compound films on the target surface during the pulse on-time when the pulse off-time is longer. These two studies confirmed that HiPIMS can eliminate/suppress the hysteresis effect and made the process more stable than DCMS.

Recently, Audronis *et al.* [52] reported characteristics of the hysteresis effect using HiPIMS as well as DCMS for the Ti-O system. The results show no difference in hysteresis width between HiPIMS and DCMS; also, pulse frequency and duty cycle only affect the overall shape of the hysteresis effect. This has been attributed to the pronounced reactive ion implantation to the target surface in reactive HiPIMS due to very high peak voltage (which leads to stronger target poisoning). It should be noted that — in contrast to Wallin and Helmersson [6] and Sarakinos *et al.* [7] — Audronis

et al. [52] used low frequencies (300, 450 and 600 Hz; the pulse on-time was 50 μ s) and a very large target area (188 mm \times 296 mm \times 9.5 mm). The material system was also different from Wallin and Helmersson [6] and Sarakinos *et al.* [7]. It should also be noted that, the measurements by Audronis *et al.* were very fast. They could record the whole hysteresis curve in only a few minutes.

At the moment, there are several explanations of the hysteresis behavior in reactive HiPIMS. We would like to focus more on this phenomenon. In **Paper 1** and **Paper 2**, we study the possibility of stabilizing the transition zone by reactive HiPIMS over a wide range of experimental parameters such as pulse frequency and duty cycle, etc. We also investigate the effect of target materials, pumping speed, target area, etc., which influences the hysteresis effect. In addition, we seek to contribute to the understanding of the fundamental mechanisms that determine the process characteristics in reactive HiPIMS processes.

3.5 Discharge Current Behavior in a Reactive HiPIMS Discharge

As described in section 2.5.2 — i.e., the discharge behavior in metal mode of HiPIMS — we found that the discharge current in a reactive HiPIMS process (using oxygen as the reactive gas) shows a pronounced difference in shape and peak value as compared to the metal mode. The discharge current waveforms in the metal (Ar) and oxide mode of HiPIMS (Ar+O₂) for (a) Ti and (b) Al sputtering targets are shown in Figure 9. It is very surprising that both Ti and Al show the same discharge current behavior in oxide mode as compared to their metal mode. This is because the change in the secondary electron yield of Ti and Al in oxide mode is different. In general, the secondary electron yield of Ti is lower in oxide mode as compared to metal mode and the opposite is true for Al [12]. In **Paper 4**, we investigate ion composition as well as ion energy distribution in both metal and oxide modes for Ti and Al. The paper contributes towards understanding the behavior.

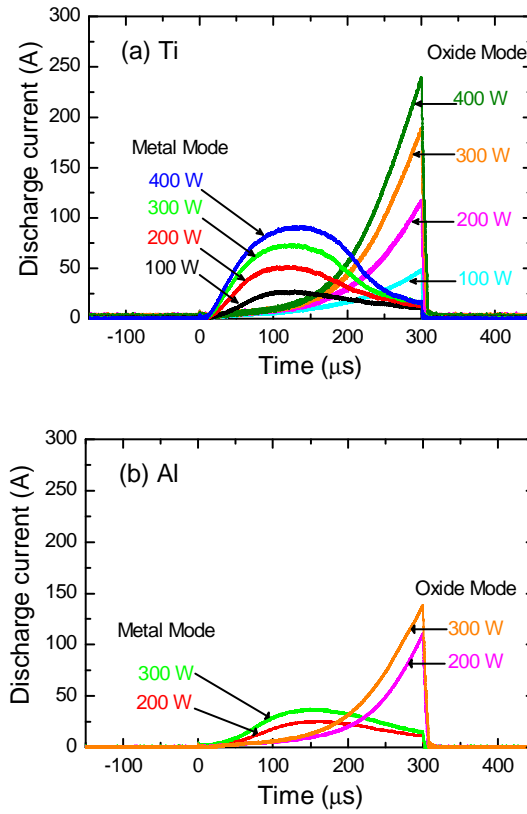


Figure 9: Typical discharge current waveforms in the metal (Ar) and oxide mode of HiPIMS ($\text{Ar}+\text{O}_2$) for (a) Ti and (b) Al sputtering targets. The pulsing frequency was constant (50 Hz), the pulse length was 300 μs , and the target diameter was 100 mm. The average discharge power was varied between 100 and 400 W.

Chapter 4

Metal Oxide Thin Film Materials

In this chapter, an overview of the material systems used in the thesis along with a brief literature survey related to the synthesis of thin films using these material systems is presented.

4.1 Al-O System

Aluminum oxide or alumina (Al_2O_3) is a ceramic material with excellent properties such as high abrasive and corrosion resistance, high hardness, chemical inertness and optical transparency [51,53–55]. However, the properties of Al_2O_3 strongly depend on the structure (amorphous or crystalline), where the crystalline Al_2O_3 can exhibit different phases, i.e., α , κ , θ , η , and γ [56, p. 30]. Among the different phases, α (corundum) is the only thermodynamically stable phase. The properties make α - Al_2O_3 suitable for use in cutting tools. Thin films synthesized by sputter deposition at room temperature are typically x-ray amorphous. Metastable phases — mostly κ , θ , and γ - Al_2O_3 — occur at a substrate temperature between 180–700°C in reactive magnetron sputtering or if any special technique during the film growth, e.g., bipolar pulse dual magnetron sputtering [54] or a RF coil is used to increase the ionization of sputtered flux [57]. Crystalline α - Al_2O_3 can be synthesized by conventional pulse DCMS at substrate temperatures approximately 760°C as demonstrated by Zywitzki *et al.* [53].

Lower substrate temperature (650°C) can be used to synthesize the α -Al₂O₃ phase using reactive HiPIMS as shown by Wallin *et al.* [51].

4.2 Ti-O System

Titanium dioxide or titania (TiO₂) is used for various applications such as optically transparent [58], photocatalytic [59,60] and photoelectrochemical [61] coatings. TiO₂ exhibits three different phases namely anatase, rutile and brookite. The crystalline structure for anatase and rutile is tetragonal [62], whereas brookite has an orthorhombic structure [62]. Conventional magnetron sputtering at room temperature produces typically x-ray amorphous films. In order to get anatase or rutile, additional heat at the substrate during deposition is required. The anatase phase is formed at lower temperature (~200°C [63]) while the rutile phase is formed at higher temperature (above 600°C [58]). Recently, anatase and rutile TiO₂ thin films deposited by reactive HiPIMS were obtained without substrate heating [64]. In **Paper 4**, synthesis of TiO₂ thin films using reactive HiPIMS is demonstrated. The results demonstrate the possibility of synthesis of anatase, rutile and mixed phases by reactive HiPIMS when the peak power is varied.

4.3 Ce-O System

Cerium oxide or ceria (CeO₂) is an electrical semiconductor oxide. It has a fluorite type cubic structure [65] with a lattice constant at room temperature of 5.411 Å. CeO₂ can be used for microelectronic semiconductor devices [66], chemical diffusion barriers [67], optical coatings [68], oxygen sensors [69] and solid electrolytes for fuel cells [70]. For thin films, many techniques are being used for fabrication of CeO₂ including, thermal evaporation [71], e-beam evaporation [72], pulse laser deposition (PLD) [73], sol-gel [74] and magnetron sputtering [70,75]. CeO₂ can be deposited directly on a silicon substrate without the need of a barrier layer due to a crystallographic match with the substrate; the lattice mismatch parameter between them is a very small value of 0.3% [76].

4.4 Ag-Cu-O System

Silver copper oxide, Ag₂Cu₂O₃, was first synthesized in powder form using a co-precipitation method and reported in 1999 by Gomez-Romero *et al.* [77]. Ag₂Cu₂O₃ has a tetragonal structure with a space group *I4₁/amd* and lattice constants $a =$

0.58857 nm and $c = 1.06868$ nm [78]. In a theoretical study, Feng *et al.* [79] predicted excellent optical and electrical properties such as a narrow band gap and a high absorption coefficient. These properties make $\text{Ag}_2\text{Cu}_2\text{O}_3$ suitable for photovoltaic applications.

Thin films of $\text{Ag}_2\text{Cu}_2\text{O}_3$ were first produced using reactive magnetron sputtering of a copper target partially covered by silver chips [78]. However, stoichiometric $\text{Ag}_2\text{Cu}_2\text{O}_3$ films were not found. In order to synthesize the stoichiometric $\text{Ag}_2\text{Cu}_2\text{O}_3$, several researches tried to use various strategies such as co-sputtering of silver and copper targets [80] as well as alloy targets — $\text{Ag}_{0.9}\text{Cu}_{0.1}$ [81], $\text{Ag}_{0.8}\text{Cu}_{0.2}$ [81], $\text{Ag}_{0.7}\text{Cu}_{0.3}$ [81], $\text{Ag}_{0.6}\text{Cu}_{0.4}$ [82] and $\text{Ag}_{0.5}\text{Cu}_{0.5}$ [83,84]. Moreover, the effect of deposition parameters such as annealing temperature [84], deposition temperature [81,83], oxygen flow rate [82] and deposition power [83] on the $\text{Ag}_2\text{Cu}_2\text{O}_3$ films properties was investigated. Uthanna *et al.* [81] and Hari *et al.* [85] found that the single phase of $\text{Ag}_2\text{Cu}_2\text{O}_3$ can be synthesized using an alloy silver-copper ($\text{Ag}_{0.7}\text{Cu}_{0.3}$). Recently, Lund *et al.* [83] have shown that the deposition temperature in the range 200 - 300°C can be used to synthesize $\text{Ag}_2\text{Cu}_2\text{O}_3$ films from an alloy silver-copper ($\text{Ag}_{0.5}\text{Cu}_{0.5}$) target. Synthesis of $\text{Ag}_2\text{Cu}_2\text{O}_3$ thin films using reactive HiPIMS is demonstrated in **Paper 5** in this thesis. The results show that the film structure measured by grazing incidence x-ray diffraction exhibits a stoichiometry very close to that of the bulk material which has previously not been demonstrated.

Chapter 5

Plasma and Film Characterization

In this chapter, a brief description of the analytical techniques used is given. The techniques are divided into two groups: plasma characterization and film characterization. The plasma characterization has been used for studying the influence of plasma chemistry and energetic on the film properties while the film properties such as optical, structural, etc., were investigated in order to seek a correlation between the plasma and film properties.

5.1 Plasma Characterization

The plasma composition, ionized fluxes of the depositing species and energy distributions of sputtered metal, reactive and sputtering gas ions were measured using time-averaged and time-resolved mass spectrometry.

5.1.1 Mass Spectrometry

The basic operation of the mass spectrometer is described as follows. The mass spectrometer can be divided into four sections [86]: an extractor probe, energy filter, mass filter and detector, as shown in Figure 10.

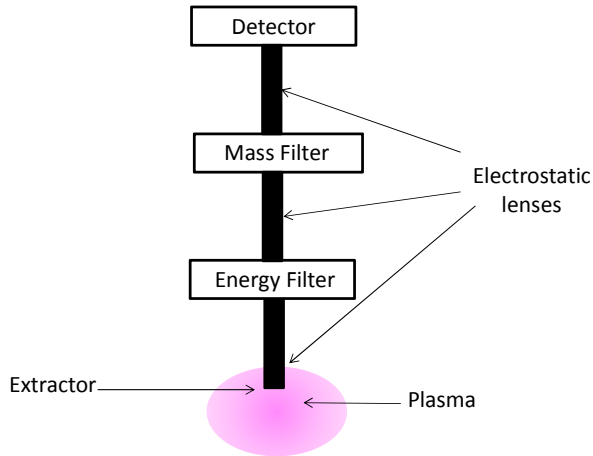


Figure 10. Schematic of a mass spectrometer.

The extractor probe with a small orifice (diameter between 50 - 300 μm) is inserted into the plasma. Neutral and ionized plasma constituents can enter into the spectrometer through the orifice. The extractor section also contains an ionization source where electron impact ionization of the neutral gas species takes place. This is used when the residual gas analysis (RGA) is desired. When measuring ions the ionization source is turned off. The ions in the extractor are focused by an electrostatic lens to the energy filter section of the spectrometer which is a so called Bessel box. Here the ions with a certain energy are selected which are then sent to the final stage of the filtering process (mass filter) using another focusing electrostatic lens. A commonly used mass filter — a quadrupole mass filter — uses four parallel electrodes which filters out the ions of undesired mass. Finally, the ions of the selected mass and energy will be detected with the detector — also called the secondary electron multiplier (or Faraday cup) detector. Typically, the distribution functions measured by a mass spectrometer represent the ion velocity distribution function in the forward direction vs. energy [86]. Ellmer *et al.* [86] have shown, using the conversion fraction, the relation between the ion velocity distribution and the ion energy distribution functions. In **Paper 3** and **Paper 4**, we reported the energy distribution functions without any conversion due to the small change of shape between velocity and energy distributions, if the energy of ions is less than 100 eV [87].

5.2 Film Characterization

In this thesis, four different techniques for the film characterization (x-ray diffractometry, spectroscopic ellipsometry, scanning electron microscope and elastic recoil detector analysis) have been used and the details of each technique are described in the following section.

5.2.1 X-ray Diffractometry

An x-ray is an electromagnetic wave with wavelength in the range of 0.01 - 10 nm. Most atoms in a solid (crystal) are arranged periodically in a lattice, and the spacing between the planes in the crystal is of the same order of magnitude of an x-ray wavelength, which makes x-rays suitable to analyze the crystallography of a crystal. A schematic illustration of $\theta/2\theta$ x-ray diffraction setup is shown in Figure 11. The angle of the primary beam and the exiting beam is θ with respect the sample surface during operating. The basic principal of x-ray diffractometry is described by Bragg's law of reflection [88, p. 10] where the path difference of beams reflected from different atomic planes is equal to an integer number of wavelengths

$$2d \sin \theta = n\lambda ,$$

where d is the spacing between the diffracted planes, θ is the incident angle of the x-ray beam, n is integer and λ is the wavelength of the x-ray. The diffraction pattern of the crystalline phase is unique and depends on the material. The peak positions in a diffractogram depend on the structure factor while the width of the peak depends on the grain/crystallite size. If the grain/crystallite size is smaller, the peak broadens. When no peak is detected by XRD, the material has very small grain size or the material is amorphous and the structure is referred to as x-ray amorphous.

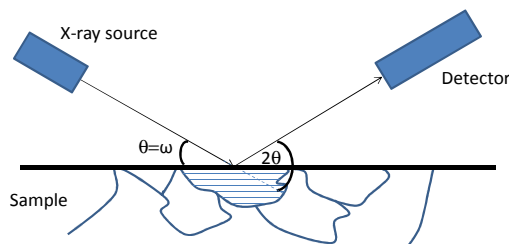


Figure 11. Schematic of $\theta/2\theta$ x-ray diffraction setup. $\theta = \omega$ is the angle of the incident beam relative to the sample surface. 2θ is the diffraction angle.

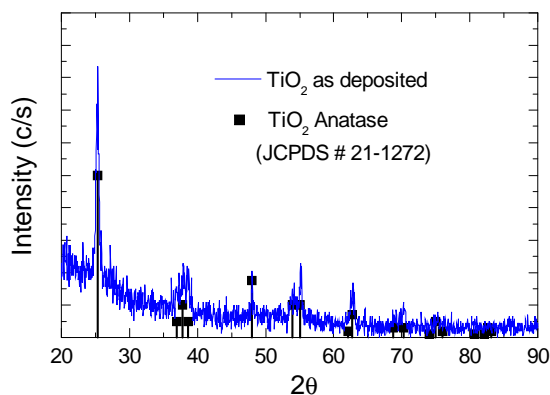


Figure 12. A grazing incidence x-ray diffractogram of TiO₂ films. The solid vertical lines show the peak position for anatase - TiO₂ (JCPDS - Joint Committee on Powder Diffraction Standards).

In this thesis, grazing incidence x-ray diffraction (GIXRD) was used to investigate the crystallography of oxide films. In this method, the incident angle of the primary beam (ω) with respect to the sample surface is kept at small angle, typically 1- 5°. Therefore, Bragg reflections are only coming from the surface structure thereby making this technique suitable for analyzing very thin films [88, p. 143-159]. Another difference in the GIXRD method compared to the $\theta/2\theta$ x-ray diffraction method is that in GIXRD, the planes in different orientations compared to the substrate surface are probed, whereas with a $\theta/2\theta$ scan only planes parallel to the substrate surface are probed [88, p. 150].

In this thesis, a Philips PW1830 diffractometer was used to perform analysis of the crystal structure. The measurements were performed with Cu K α ($\lambda = 0.15406$ nm) monochromatic radiation operated at 40 keV and 40 mA. In **Paper 1**, the incident beam angle, ω , was 1° while the scanning range in 2θ was 15 - 85°. In **Paper 4**, the incident beam angle, ω , was 3° while the scanning range in 2θ was 20 - 65°. An example of a GIXRD pattern of an anatase TiO₂ thin film is shown in Figure 12. In **Paper 5**, the crystal structure was measured by a Philips X'Pert MRD diffractometer with Cu K α ($\lambda = 0.15406$ nm) monochromatic radiation operated at 40 kV and 40 mA. The incident beam angle, ω , was 1° while the scanning range in 2θ was 15 - 85°.

5.2.2 Spectroscopic Ellipsometry

Ellipsometry is a technique used to investigate optical properties. This technique is surface sensitive and non-destructive. In ellipsometry, the change of polarization of light upon reflection is measured. In general, when a polarized light beam impinges the sample surface and reflects, the polarization changes depending on the properties of the sample. Typical parameters which are measured are Ψ and Δ where Ψ describes the relative amplitude change and Δ represents the relative phase change upon reflection [2, p. 573]. The schematic view of a spectroscopic ellipsometer setup is shown in Figure 13.

In this work, the optical properties and thickness of the thin films were investigated by utilizing ellipsometric parameters (Ψ and Δ) measured by a dual rotating compensator ellipsometer (RC2) from J. A. Woollam Co., Inc. The recorded Ψ and Δ spectra were analyzed using the CompleteEASE software from J. A. Woollam Co., Inc. by fitting the data to a model consisting of an Al-O layer on a Si substrate. The optical response of the Al-O layer (refractive index, n , and extinction coefficient, k) was described using the Cauchy dispersion formula; the results are shown in **Paper 1** of a model consisting of a Ti-O layer on a Si substrate. The optical response of the Ti-O layer (refractive index, n , and extinction coefficient, k) was described using the Cauchy dispersion formula and the results are shown in **Paper 4**.

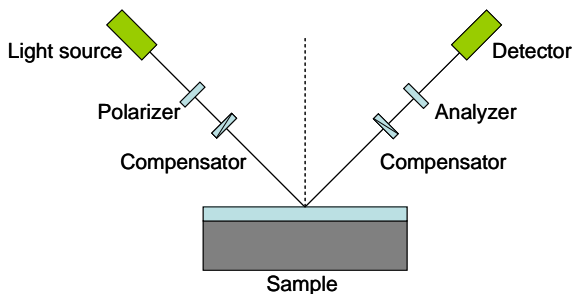


Figure 13. Schematic view of spectroscopic ellipsometry.

5.2.3 Scanning Electron Microscopy

In scanning electron microscopy (SEM) an electron beam is employed to illuminate the sample and the backscattered and secondary electrons ejected from the sample are collected to form an image. The electron beam is produced by heating a metallic filament (a type of electron source). The electron beam is focused by electromagnetic lenses which direct the beam down to the sample surface. The electron beam can be accelerated to energies ranging from 0.5 - 50 keV [2, p. 585]. When the electron beam hits the sample surface, electrons in the beam can penetrate and lose energy due to scattering and absorption within a pear-shaped volume inside the sample. The size of the pear-shaped volume is dependent on the electron energy, atomic number of the sample element and the sample density. The interaction between the electron beam and the sample leads to an energy exchange between; this results in the reflection of high energy electrons (backscattered electron), emission of secondary electrons and emission of electromagnetic radiation [2, p. 586-589]. In general, the sample should be electrically conductive to prevent the accumulation of electrostatic charge at the surface. However, a non-conductive sample can be analyzed via SEM using special preparation routine. The special preparation usually involves coating the sample with an ultrathin electrically-conducting material, commonly gold. This coating can prevent the accumulation of static electrical charge on the sample during electron irradiation. In this work, SEM was used to look at a sample cross section to measure the film thickness. The samples in this work such as Al_2O_3 and TiO_2 are non-conductive. In this thesis we used low energy (3 keV) electron beam instead of coating the samples with ultrathin gold in order to lower the risks of build-up of static electric charge.

5.2.4 Elastic Recoil Detector Analysis

In order to investigate the chemical composition and element depth profiles in the near surface layer of thin films, ion beam analysis can be employed. Elastic recoil detection analysis (ERDA) is an ion beam based analysis technique which is used for quantitative analysis of light to medium elements [89]. ERDA uses a heavy ion beam with energy in the order of several MeV. The incoming beam knocks out atoms in the sample and the recoiled atoms are picked up by the detector. Typical scattering geometry is shown in Figure 14. When a projectile of mass M_1 , atomic number Z_1 , and energy E_1 collides with an atom of mass M_2 and atomic number Z_2 in the sample,

it will transfer the energy E_2 to the atom at a recoil angle θ . From the measured energy spectrum of the recoil, a concentration depth profile can be calculated. In this work, the film stoichiometry was determined by means of time-of-flight elastic recoil detection analysis (ToF-ERDA). 40 MeV $^{127}\text{I}^{9+}$ ions were used as a projectile beam and the incident angle relative to the surface was 22.5° . The detector was placed at a recoil scattering angle of 45° . In **Paper 1** and **Paper 4**, we used ERDA to determine the film compositions.

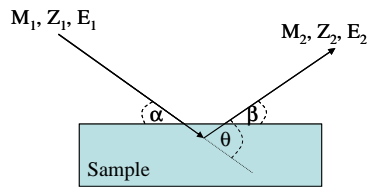


Figure 14. Schematic of the ERDA geometry.

Chapter 6

Summary of Results

In this chapter I will summarize the main results of the five included papers and share my opinion on how this thesis may have contributed to the field of reactive sputtering. I have conducted research on metal oxides deposited by reactive high power impulse magnetron sputtering (HiPIMS). Understanding process behavior of reactive HiPIMS is one of the major ways for improving the deposition process, deposition rate, process stability and film properties. Direct current magnetron sputtering (DCMS) was also studied as a comparison to reactive HiPIMS under the similar conditions.

6.1 Fundamentals of Reactive High Power Impulse Magnetron Sputtering

Paper 1 - Hysteresis and process stability in reactive high power impulse magnetron sputtering of metal oxides

Al-O and Ce-O systems were used to study the hysteresis effect by reactive HiPIMS and DCMS. It was found that for the same sputtering conditions, reactive HiPIMS can eliminate/reduce the hysteresis effect in comparison to DCMS. The stabilization of the transition zone is observed in the range of frequency (2 and 4 kHz) for Al-O while for Ce-O, reactive HiPIMS can reduce the hysteresis effect. The main mechanism proposed to explain this phenomenon is the effect of gas rarefaction and refill time of

the gas dynamic between the pulses. Moreover, it was found that the stabilization of the transition zone in HiPIMS is not dependent on the pumping speed of the system. In order to unravel the effect of the process stability on the film properties, Al₂O₃ films were grown on Si substrates by reactive HiPIMS and DCMS. A series of films with thicknesses of about 200 nm was grown varying the oxygen gas flows. Again, HiPIMS showed a wide stable range to grow the stoichiometric films and the deposition rate of the films were higher than DCMS. Furthermore, the properties of films deposited by reactive HiPIMS showed a higher refractive index indicating higher film density as compared to films deposited by reactive DCMS.

Paper 2 - Studies of hysteresis effect in reactive HiPIMS deposition of oxides

The effect of target area on the hysteresis effect in reactive HiPIMS was investigated in this work. A Ti-O system was used and the diameter of the Ti target was 100 mm. The geometry of the system is also different from the system in **Paper 1** in order to compare the characteristic hysteresis curve as related to pulse frequency for different geometry systems. The results show that although the geometry of the system is different, reactive HiPIMS can reduce the hysteresis width; also, there is an optimum frequency to minimize the hysteresis width. The effect of gas rarefaction and gas refill times are also investigated. The gas rarefaction in front of the target starts to dominate when the off-time is short enough to prevent the gas refill in front of the target. Furthermore, gas rarefaction is more pronounced with increasing peak current. In summary, this paper indicates that the reduction of the hysteresis effect may be very system dependent.

Paper 3 - Understanding the discharge current behavior in reactive high power impulse magnetron sputtering of oxides

In this paper, differences in the discharge current behavior in non-reactive and reactive high power impulse magnetron sputtering of metal oxides, i.e. different shapes and peak current density, are studied. This work contributes towards understanding the physics of reactive high power impulse magnetron sputtering (HiPIMS) processes by studying the discharge current behavior of Ti-O and Al-O. The understanding was developed by investigating the ionic contributions as well as the time evolution of the sputtering and reactive gas ions (Ar¹⁺ and O¹⁺ respectively) and sputtered metal ions (Ti¹⁺ and Al¹⁺) to the discharge current. The effect of

secondary electron emission yield of metal and oxide target surfaces along with the influence of the partial sputtering yields for Ar^{1+} , Ti^{1+} , Al^{1+} and O^{1+} on the discharge current were also investigated. It was found that in a reactive HiPIMS process, the discharge was dominated by ionized oxygen and the energy distribution functions of the O^{1+} ions resemble to that of the sputtered metal. It was established that the oxygen is preferentially sputtered from the target surface which means that the source of O^{1+} ions was the sputtering target rather than the gas phase. The ionized oxygen determines the discharge behavior in reactive HiPIMS, and its contribution to the observed increased discharge currents in oxide mode is vital. Another important finding of this paper is the observation that a strong gas depletion regime is never reached when operating in the oxide mode. The experimental observations of this research were also supported by TRIDYN simulations.

6.2 Growth Using Reactive High Power Impulse Magnetron Sputtering

Paper 4 - Effect of peak power in reactive high power impulse magnetron sputtering of titanium dioxide

In this paper, the effect of peak power on the properties of TiO_2 films grown by reactive HiPIMS and DCMS was investigated. For constant average power and pulse on-time, the change in pulse frequency led to a change in the peak power. That is, the peak power increased with decreased pulse frequency. It was found that it was possible to control the phase composition via the HiPIMS peak power, and films containing pure anatase, pure rutile and a mixture between anatase and rutile phases were grown. Furthermore, the ion composition and their energy distributions were analyzed using energy resolved mass spectrometry. The ion energy distributions showed that O ions in the plasma were more energetic than the Ti ions. The crystallinity and variation in the phase composition of TiO_2 films depended on the energy of the arriving particles (mainly ionized species). TiO_2 films deposited by reactive HiPIMS showed superior properties to the films deposited by DCMS, i.e., a higher refractive index and a higher film density. The deposition rate is a small lost in HiPIMS as compared to DCMS.

Paper 5 - $\text{Ag}_2\text{Cu}_2\text{O}_3$ films deposited by reactive high power impulse magnetron sputtering

In this paper, the effect of peak power investigated in **Paper 4** was studied for a new material system, where the target is an alloy (Ag/Cu). In this study, the influence of peak power and oxygen gas flow rate on the film structure is investigated using reactive HiPIMS as well as DCMS. It was found that the films deposited by HiPIMS, in order to get stoichiometric $\text{Ag}_2\text{Cu}_2\text{O}_3$ films, required higher oxygen gas flow when increasing peak power. This may be due to target cleaning efficiency during the pulse and re-sputtering effect at the substrate with highly energetic incoming species especially, negative oxygen ions. It is also found that the stoichiometric $\text{Ag}_2\text{Cu}_2\text{O}_3$ films deposited by HiPIMS can be grown at room temperature with pronounced crystalline structures than DCMS while the deposition rates are comparable in both cases.

References

- [1] K. S. Sree Harsha, *Principles of Physical Vapor Deposition of Thin Films*, Elsevier Science, Oxford (2006).
- [2] M. Ohring, *Materials Science of Thin Films*, 2nd ed., Academic Press, San Diego, (2002).
- [3] W. D. Sproul, D. J. Christie, D. C. Carter, *Thin Solid Films* **491** (2005) 1.
- [4] J. Musil, P. Baroch, J. Vlcek, K. H. Nam, J. G. Han, *Thin Solid Films* **475** (2005) 208.
- [5] S. Berg, T. Nyberg, *Thin Solid Films* **476** (2005) 215.
- [6] E. Wallin, U. Helmersson, *Thin Solid Films* **516** (2008) 6398.
- [7] K. Sarakinos, J. Alami, C. Klever, M. Wuttig, *Surf. Coat. Technol.* **202** (2008) 5033.
- [8] I. Langmuir, *Physical Review* **33** (1929) 954.
- [9] M. A. Lieberman, A. J. Lichtenberg, *Principles of Plasma Discharges and Materials Processing*, 2nd ed., John Wiley & Sons, New Jersey (2005).
- [10] J. R. Roth, *Industrial Plasma Engineering Volume 1: Principles*, Institute of Physics Publishing, Bristol, UK, (1995).
- [11] Y. Okajima, *J. Appl. Phys.* **51** (1980) 715.
- [12] D. Depla, S. Heirwegh, S. Mahieu, J. Haemers, R. De Gryse, *J. Appl. Phys.* **101** (2007) 013301.
- [13] P. J. Kelly, R. D. Arnell, *Vacuum* **56** (2000) 159.
- [14] P. M. Martin, ed., *Handbook of Deposition Technologies for Films and Coatings*, 3rd ed., Elsevier, William Andrew, Oxford, (2009).
- [15] U. Helmersson, M. Lattemann, J. Bohlmark, A. P. Ehasarian, J. T. Gudmundsson, *Thin Solid Films* **513** (2006) 1.
- [16] V. Kouznetsov, K. Macak, J. M. Schneider, U. Helmersson, I. Petrov, *Surf. Coat. Technol.* **122** (1999) 290.
- [17] A. P. Ehasarian, R. New, W. -D. Munz, L. Hultman, U. Helmersson, V. Kouznetsov, *Vacuum* **65** (2002) 147.
- [18] J. Alami, P. O. Å. Persson, D. Music, J. T. Gudmundsson, J. Bohlmark, U. Helmersson, *J. Vac. Sci. Technol. A* **23** (2005) 278.

- [19] J. Bohlmark, M. Östbye, M. Lattemann, H. Ljungcrantz, T. Rosell, U. Helmersson, *Thin Solid Films* **515** (2006) 1928.
- [20] M. Samuelsson, D. Lundin, J. Jensen, M. A. Raadu, J. T. Gudmundsson, U. Helmersson, *Surf. Coat. Technol.* **205** (2010) 591.
- [21] J. Alami, P. Eklund, J. M. Andersson, M. Lattemann, E. Wallin, J. Bohlmark, P. Persson, U. Helmersson, *Thin Solid Films* **515** (2007) 3434.
- [22] A. P. Ehiasarian, P. Eh. Hovsepien, L. Hultman, U. Helmersson, *Thin Solid Films* **457** (2004) 270.
- [23] J. Alami, P. Eklund, J. Emmerlich, O. Wilhelmsson, U. Jansson, H. Högberg, L. Hultman, U. Helmersson, *Thin Solid Films* **515** (2006) 1731.
- [24] A. P. Ehiasarian, W. -D. Munz, L. Hultman, U. Helmersson, I. Petrov, *Surf. Coat. Technol.* **163-164** (2003) 267.
- [25] Y. P. Purandare, A. P. Ehiasarian, P. Eh. Hovsepien, *J. Vac. Sci. Techn. A* **26** (2008) 288.
- [26] A. P. Ehiasarian, J. G. Wen, I. Petrov, *J. Appl. Phys.* **101** (2007) 054301.
- [27] K. Sarakinos, J. Wördenweber, F. Uslu, P. Schulz, J. Alami, M. Wuttig, *Surf. Coat. Technol.* **202** (2008) 2323.
- [28] A. Anders, J. Andersson, A. Ehiasarian, *J. Appl. Phys.* **102** (2007) 113303.
- [29] A. Anders, G. Yu. Yushkov, *J. Appl. Phys.* **105** (2009) 073301.
- [30] D. W. Hoffman, *J. Vac. Sci. Technol. A* **3** (1985) 561.
- [31] S. M. Rosnagel, *J. Vac. Sci. Technol. B* **16** (1998) 3008.
- [32] S. Kadlec, *Plasma Processes Polym.* **4** (2007) S419.
- [33] D. Lundin, N. Brenning, D. Jädernäs, P. Larsson, E. Wallin, M. Lattemann, M. A. Raadu, U. Helmersson, *Plasma Sources Sci. Technol.* **18** (2009) 045008.
- [34] K. Sarakinos, J. Alami, S. Konstantinidis, *Surf. Coat. Technol.* **204** (2010) 1661.
- [35] D. J. Christie, *J. Vac. Sci. Technol. A* **23** (2005) 330.
- [36] D. Lundin, P. Larsson, E. Wallin, M. Lattemann, N. Brenning, U. Helmersson, *Plasma Sources Sci. Technol.* **17** (2008) 035021.
- [37] S. P. Bugaev, N. N. Koval, N. S. Sochugov, A. N. Zakharov, *Proceedings of the XVIIth International Symposium on Discharges and Electrical Insulation in Vacuum*, Berkeley, CA, (1996) 1074.
- [38] J. A. Thornton, *Ann. Rev. Mater. Sci.* **7** (1977) 239.

- [39] S. Schiller, U. Heisig, K. Steinfeld, J. Strumpf, R. Voigt, R. Fendler, G. Teschner, *Thin Solid Films* **96** (1982) 235.
- [40] J. Affinito, R. R. Parsons, *J. Vac. Sci. Technol. A* **2** (1984) 1275.
- [41] R. Ramamoorthy, P. K. Dutta, S. A. Akbar, *J. Mater. Sci.* **38** (2003) 4271.
- [42] P. J. Kelly, P. S. Henderson, R. D. Arnell, G. A. Roche, D. Carter, *J. Vac. Sci. Technol. A* **18** (2000) 2890.
- [43] S. Kadlec, J. Musil, J. Vyskocil, *Vacuum* **37** (1987) 729.
- [44] T. Nyberg, S. Berg, U. Helmersson, K. Hartig, *Appl. Phys. Lett.* **86** (2005) 164106.
- [45] T. Kubart, D. Depla, D. M. Martin, T. Nyberg, S. Berg, *Appl. Phys. Lett.* **92** (2008) 221501.
- [46] D. Severin, O. Kappertz, T. Kubart, T. Nyberg, S. Berg, A. Pflug, M. Siemers, M. Wuttig, *Appl. Phys. Lett.* **88** (2006) 161504.
- [47] M. Lattemann, U. Helmersson, J. E. Greene, *Thin Solid Films* **518** (2010) 5978.
- [48] K. Sarakinos, J. Alami, M. Wuttig, *J. Phys. D: Appl. Phys.* **40** (2007) 2108.
- [49] S. Konstantinidis, J. P. Dauchot, M. Hecq, *Thin Solid Films* **515** (2006) 1182.
- [50] S. Konstantinidis, A. Hemberg, J. P. Dauchot, M. Hecq, *J. Vac. Sci. Technol. B* **25** (2007) L19.
- [51] E. Wallin, T. I. Selinder, M. Elfving, U. Helmersson, *Europhys. Lett.* **82** (2008) 36002–p1.
- [52] M. Audronis, V. B. Gonzalez, *Thin Solid Films* **518** (2010) 1962.
- [53] O. Zywitzki, G. Hoetzsch, F. Fietzke, K. Goedicke, *Surf. Coat. Technol.* **82** (1996) 169.
- [54] M. Åstrand, T. I. Selinder, F. Fietzke, H. Klostermann, *Surf. Coat. Technol.* **188-189** (2004) 186.
- [55] K. Koski, J. Hölsä, P. Juliet, *Thin Solid Films* **339** (1999) 240.
- [56] W. H. Gitzen, *Alumina as a Ceramic Material*, The American Ceramic Society, Westerville, 1970.
- [57] J. M. Schneider, W. D. Sproul, A. A. Voevodin, A. Matthews, *J. Vac. Sci. Technol. A* **15** (1997) 1084.
- [58] L. Miao, P. Jin, K. Kaneko, A. Terai, N. Nabatova-Gabain, S. Tanemura, *Appl. Surf. Sci.* **212-213** (2003) 255.
- [59] K. Sunada, *Environ. Sci. Technol.* **32** (1998) 726.

- [60] A. Fujishima, T. N. Rao, D. A. Tryk, J. Photochem. Photobiol. C **1** (2000) 1.
- [61] T. Lindgren, J. M. Mwabora, E. Avendano, J. Jonsson, A. Hoel, C. G. Granqvist, S. E. Lindquist, J. Phys. Chem. B **107** (2003) 5709.
- [62] M. D. Wiggins, M. C. Nelson, C. R. Aita, J. Vac. Sci. Technol. A **14** (1996) 772.
- [63] D. Wicaksana, A. Kobayashi, A. Kinbara, J. Vac. Sci. Technol. A **10** (1992) 1479.
- [64] V. Straňák, M. Quaas, H. Wulff, Z. Hubička, S. Wrehde, M. Tichý, R. Hippler, J. Phys. D: Appl. Phys. **41** (2008) 055202.
- [65] M. Mogensen, N. M. Sammes, G. A. Tompsett, **129** (2000) 63.
- [66] L. Tye, N. A. El-Masry, T. Chikyow, P. Mclarty, S. M. Bedair, Appl. Phys. Lett. **65** (1994) 3081.
- [67] F. C. Fonseca, S. Uhlenbruck, R. Nédélec, D. Sebold, H. P. Buchkremer, J. Electrochem. Soc. **157** (2010) B1515.
- [68] S. Kanakaraju, S. Mohan, A. K. Sood, Thin Solid Films **305** (1997) 191.
- [69] P. Jasinski, T. Suzuki, H. U. Anderson, Sens. Actuators, B **95** (2003) 73.
- [70] Y.-L. Kuo, C. Lee, Y.-S. Chen, H. Liang, Solid State Ionics **180** (2009) 1421.
- [71] V. Matolín, J. Libra, I. Matolínová, V. Nehasil, L. Sedláček, F. Šutara, Appl. Surf. Sci. **254** (2007) 153.
- [72] T. Inoue, Y. Yamamoto, M. Satoh, Thin Solid Films **343-344** (1999) 594.
- [73] V. Trtik, R. Aguiar, F. Sanchez, C. Ferrater, M. Varela, **192** (1998).
- [74] N. Özer, Sol. Energy Mater. Sol. Cells **68** (2001) 391.
- [75] L. Kim, J. Kim, D. Jung, C. Y. Park, C. W. Yang, Y. Roh, Thin Solid Films **360** (2000) 154.
- [76] O. Nakagawara, M. Kobayashi, Y. Yoshino, Y. Katayama, H. Tabata, T. Kawai, J. Appl. Phys. **78** (1995) 7226.
- [77] P. Gomez-Romero, E. M. Tejada-Rosales, M. Rosa Palacin, Angew. Chem. Int. Ed. **38** (1999) 524.
- [78] J. F. Pierson, D. Wiederkehr, J.-M. Chappé, N. Martin, Appl. Surf. Sci. **253** (2006) 1484.
- [79] J. Feng, B. Xiao, J. C. Chen, C. T. Zhou, Y. P. Du, R. Zhou, Solid State Commun. **149** (2009) 1569.
- [80] J. F. Pierson, D. Horwat, Appl. Surf. Sci. **253** (2007) 7522.

- [81] S. Uthanna, M. H. P. Reddy, P. Boulet, C. Petitjean, J. F. Pierson, *Phys. Status Solidi A* **207** (2010) 1655.
- [82] J. F. Pierson, E. Rolin, C. Clément-Gendarme, C. Petitjean, D. Horwat, *Appl. Surf. Sci.* **254** (2008) 6590.
- [83] E. Lund, A. Galeckas, E. V. Monakhov, B. G. Svensson, *Thin Solid Films* **520** (2011) 230.
- [84] C. Petitjean, D. Horwat, J. F. Pierson, *Appl. Surf. Sci.* **255** (2009) 7700.
- [85] M. Hari Prasad Reddy, J. F. Pierson, S. Uthanna, *Cryst. Res. Technol.* **46** (2011) 1329.
- [86] K. Ellmer, R. Wendt, K. Wiesemann, *Int. J. Mass Spectrom.* **223-224** (2003) 679.
- [87] S. Seeger, K. Harbauer, K. Ellmer, *J. Appl. Phys.* **105** (2009) 053305.
- [88] M. Birkholz, *Thin Film Analysis by X-Ray Scattering*, Wiley-VCH, Weinheim, (2006).
- [89] D. D. Cohen, R. Bird, N. Dytlewski, R. Siegele, *Encycl. Phys. Sci. & Technol.*, Academic Press, (2001).